Nuclear Inst. and Methods in Physics Research, A 982 (2020) 164486

Contents lists available at ScienceDirect

Nuclear Inst. and Methods in Physics Research, A

journal homepage: www.elsevier.com/locate/nima

Status of the development of NUV SiPMs for INFN optical modules for the SCT medium sized telescope proposed for the CTA observatory

C. Adams [j], G. Ambrosi [a], M. Ambrosio [b], C. Aramo [b], W. Benbow [k], B. Bertucci [a,e], E. Bissaldi [c,d], M. Bitossi [f], A. Boiano [b], C. Bonavolontá [b,g], R. Bose [l], A. Brill [j], J.H. Buckley [l], M. Caprai [a], C.E. Covault [m], L. Di Venere [c,d], Q. Feng [n], E. Fiandrini [a,e], A. Gent [o], N. Giglietto [c,d], F. Giordano [c,d], R. Halliday [m], O. Hervet [p], G. Hughes [k], T.B. Humensky [j], M. Ionica [a], W. Jin [q], P. Kaaret [r], D. Kieda [s], B. Kim [t], F. Licciulli [c], S. Loporchio [c,d,*], V. Masone [b], T. Meures [u], B.A.W. Mode [u], R. Mukherjeek [n], A. Okumura [v], N. Otte [o], F.R. Pantaleo [c,d], R. Paoletti [f,h], A. Petrashyk [j], J. Powell [q], K. Powell [o], D. Riberio [j], J. Rouselle [w], A. Rugliancich [f,h], M. Santander [q], R. Shang [t], B. Stevenson [t], L. Stiaccini [f,h], L.P. Taylor [u], L. Tosti [a,e], V. Vagelli [a,x], M. Valentino [i], J. Vandenbroucke [u], V. Vassiliev [t], P. Wilcox [r], D.A. Williams [p], for the CTA pSCT project [1]

[a] INFN Sezione di Perugia, 06123 Perugia, Italy
[b] INFN Sezione di Napoli, 80126 Napoli, Italy
[c] INFN Sezione di Bari, 70125 Bari, Italy
[d] Dipartimento Interateneo dell'Università e del Politecnico di Bari, 70125 Bari, Italy
[e] Università degli Studi di Perugia, 06123 Perugia, Italy
[f] INFN Sezione di Pisa, 56127 Pisa, Italy
[g] Università degli Studi di Napoli, 80126 Napoli, Italy
[h] Dipartimento di Scienze Fisiche, della Terra e dell'Ambiente, Università degli Studi di Siena, 53100 Siena, Italy
[i] CNR-ISASI, Italy
[j] Physics Department, Columbia University, New York, NY 10027, USA
[k] Center for Astrophysics - Harvard & Smithsonian, Cambridge, MA 02138, USA
[l] Department of Physics, Washington University, St. Louis, MO 63130, USA
[m] Department of Physics, Case Western Reserve University, Cleveland, OH 44106, USA
[n] Department of Physics and Astronomy, Barnard College, Columbia University, NY 10027, USA
[o] School of Physics & Center for Relativistic Astrophysics, Georgia Institute of Technology, 837 State Street NW, Atlanta, GA 30332-0430, USA
[p] Santa Cruz Institute for Particle Physics and Department of Physics, University of California, Santa Cruz, CA 95064, USA
[q] Department of Physics and Astronomy, University of Alabama, Tuscaloosa, AL 35487, USA
[r] Department of Physics and Astronomy, University of Iowa, Iowa City, IA 52242, USA
[s] Department of Physics and Astronomy, University of Utah, Salt Lake City, UT 84112, USA
[t] Department of Physics and Astronomy, University of California, Los Angeles, CA, USA
[u] Department of Physics and Wisconsin IceCube Particle Astrophysics Center, University of Wisconsin, Madison, WI 53706, USA
[v] Institute for Space-Earth Environmental Research and Kobayashi-Maskawa Institute for the Origin of Particles and the Universe, Nagoya University, Nagoya 464-8601, Japan
[w] Subaru Telescope NAOJ, Hilo, HI 96720, USA
[x] ASI Agenzia Spaziale Italiana, 00133 Roma, Italy

ARTICLE INFO

Keywords:
SiPM
Cherenkov telescopes
Photo detectors

ABSTRACT

Near UltraViolet High Density (NUV-HD) SiPMs produced by Fondazione Bruno Kessler in collaboration with INFN have been tested and characterized in INFN laboratories. The third generation of these devices (HD3) has proven to be suitable to equip the focal plane of the prototype Schwarzschild–Couder Medium Size Telescope (pSCT) proposed for the Cherenkov Telescope Array Observatory. Photosensors have been assembled in 4 16-pixel optical units coupled with TARGET–7 ASIC front-end electronics for amplification and digitization of the signal. At present, 9 modules have been successfully integrated on the pSCT camera and are currently taking data. In this contribution we report on the performances of the HD3 technology as single sensor and as assembled optical units, showing their performance and homogeneity in terms of gain and dark count rate.

* Corresponding author.
E-mail address: serena.loporchio@ba.infn.it (S. Loporchio).
[1] See www.cta-observatory.org for full author & affiliation list.

https://doi.org/10.1016/j.nima.2020.164486
Received 28 November 2019; Received in revised form 9 June 2020; Accepted 28 July 2020
Available online 6 August 2020
0168-9002/

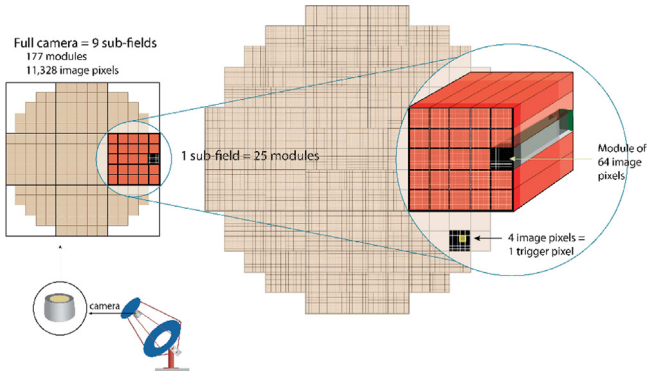

Fig. 1. Schematic of camera focal plane configuration, divided into 9 sectors backplanes. Fully loaded subfields include 25 modules of 64 pixels divided in 4 matrices of 16 SiPMs. Groups of 4 pixels compose one trigger pixel [3].

1. Introduction

Cherenkov Telescope Array (CTA) will be the largest ground-based gamma-ray observatory for very high energy gamma rays [1]. In order to provide full-sky coverage, CTA telescopes will be installed in two sites, one in the northern hemisphere (La Palma, Canary Island (s) and one in the southern hemisphere (Atacama desert, Chile). CTA will be equipped with ~100 telescopes in three different size configurations: Large, Medium and Small-Sized Telescopes (LST, MST and SST).

The Schwarzschild–Couder Telescope (SCT) is a possible dual-mirror solution for the Medium Size Telescope. A prototype SCT (pSCT) was installed at the Fred Lawrence Whipple Observatory (FLWO)[2] in Arizona, USA, and has been inaugurated in January 2019. The pSCT is demonstrating the technical feasibility of the new design and it is providing important information on the procedures for the optical alignment and for the camera operation and calibration. The usage of a double mirror optical system will provide compensation of optical aberrations, along with an improvement of the angular resolution and background rejection and wider Field of View (FoV) than the single mirror Davies–Cotton optical system [2].

2. The Schwarzschild–Couder Telescope camera

The two segmented mirrors are 9.7 and 5.4 m wide in diameter. The SCT camera, positioned in the focal plane of the secondary mirror, has a width of 0.81 m and covers a field of view of 8°, which is the same covered by the DC-MST with its 2.5 m camera. The compactness of the SCT camera is a consequence of the demagnifying optics; an advantage of the smaller camera is the possibility to equip it with silicon photomultipliers (SiPMs), in place of the photomultipliers tubes (PMTs), which are typically adopted in Imaging Air Cherenkov Telescopes. SiPMs have several advantages compared to PMTs, such as an improved mechanical and electrical robustness. The SCT camera will be composed of 11,328 SiPMs organized in 177 modules, divided in 9 sub-fields each hosting up to 25 modules, as shown in the schematic reported in Fig. 1.

A single photodetection module consists of two parts: the focal plane modules (FPM), which hosts 64 SiPMs pixels arranged in four matrices of 16 SiPMs of 6 × 6 mm^2 size, and the front-end electronics (FEE) composed of two boards, hosting 4 TARGET–7 ASIC (TeV Array Readout with GSa/s sampling and Event Trigger) each one providing digitization of the analogue signal and the first level trigger, as shown in Fig. 2.

Each ASIC is a 16 parallel input channels digitizer chip whose compact design has been optimized to match the high density pixel

[2] https://www.cfa.harvard.edu/flwo

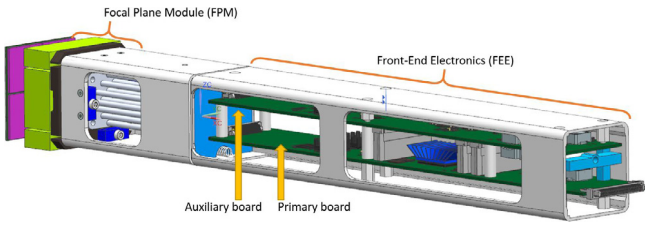

Fig. 2. Schematic of the pSCT camera module divided into an FPM (front) and a FEE (rear) parts. Between the two, the peltier cooling is visible through the opening of the metal cage. Inside the casing, the FEE module is divided into an Auxiliary and a Primary board [4].

camera of CTA telescopes [5,6]. The TARGET–7 is based on an analogue sampling memories technology which consists in a ring buffer of switched capacitors used in turn to record the signal waveform at a given sampling rate (1 GSample/second); it has an analogue ring buffer of 2^{14} = 16,384 capacitors for a sampling depth of about 16 μs, which allows the sampled waveform to be stored waiting for the trigger to be generated using the synchronized information from other telescopes of the array. By using SiPMs coupled with the TARGET–7 electronics a wide dynamic range is achieved, up to several hundred of photons.

The prototype of the Schwarzschild–Couder Telescope is now equipped with 25 64-pixel photodetection modules. To define the technology of the camera, sixteen of these modules are based on Hamamatsu S12642 MPPCs Silicon Photomultiplier (SiPM) sensors, produced and assembled in the USA. The remaining 9 have been equipped with the third generation of Near UltraViolet High Density (NUV-HD3) SiPMs produced by Fondazione Bruno Kessler (FBK), optimized for the Near UltraViolet light detection, which have been studied and assembled into matrices in Italy by the Istituto Nazionale di Fisica Nucleare (INFN).

In the following sections a complete characterization of these devices will be described, which was performed in INFN laboratories.

3. FBK NUV-HD3 SiPM characterization

A Research and Development process in collaboration between INFN and FBK led to the development of a Low Cross-Talk SiPM version, NUV-HD3 SiPM [7]. NUV-HD3 1 × 1 mm^2 and 6 × 6 mm^2 devices with a microcell area of 40 × 40 μm^2 were studied with dedicated electronics before the assembly of the matrices for the pSCT camera.

First, the characteristic voltage–current (IV) curves of single SiPMs were acquired in order to evaluate the breakdown voltage of the devices [8]; the value of the breakdown is estimated with a fit procedure on the derivative of the logarithm of the current $I = I(V)$ with the following Equation:

$$\frac{\partial \log(I(V))}{\partial V} = \frac{2}{V - V_b} \quad (1)$$

At room temperature, we obtained the value $V_{bd} = 25.88 \pm 0.01$ V for the 1 × 1 mm^2 SiPM and the value 25.55 ± 0.01 V for the 6 × 6 mm^2 device.

Then the SiPMs were characterized by acquiring waveforms in light and dark conditions, with temperature ranging between −20 °C and 30 °C and applied over-voltage (OV) ranging between ~2 V and ~13 V. We illuminated each sensor with a picosecond laser emitting at 380 nm operating in pulse mode and controlled by a Pulse Diode Laser Driver (PDL 800-B, PicoQuant). The read-out electronics used for the characterization described in this section consists of a trans-impedance preamplifier followed by a gain stage.

An example of waveforms acquired in light conditions is reported in Fig. 3 for the 1 × 1 mm^2 SiPM at 20 °C and 5.5 V of OV.

The acquired waveforms were integrated up to 300 ns to evaluate the collected charge spectrum, shown in Fig. 4: the spectrum of the

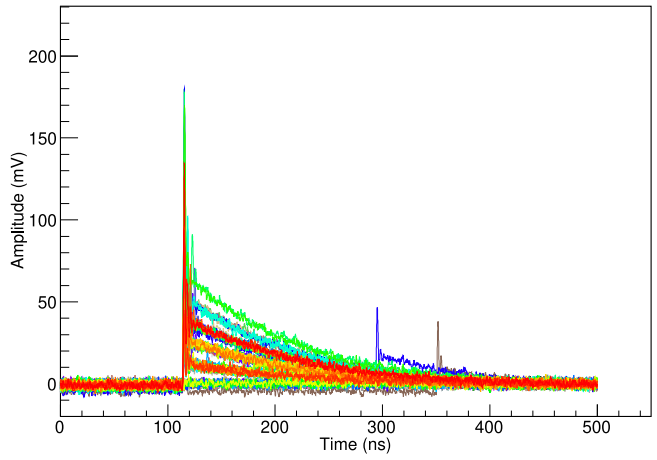

Fig. 3. Waveforms acquired for FBK NUV-HD3 1 × 1 mm^2 SiPM at OV = 5.5 V and T = 20 °C.

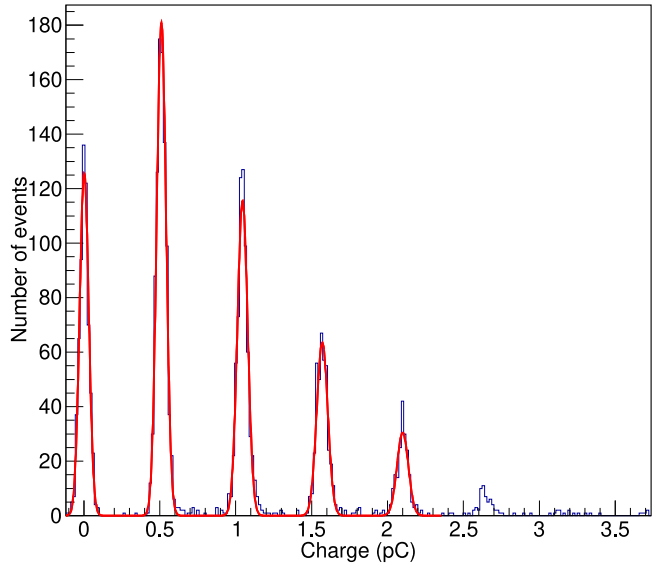

Fig. 4. Integrated charge distribution of the signal of FBK NUV-HD3 1 × 1 mm^2 SiPM shown in 3. A multi-gaussian fit is shown superimposed on data. The area of the peaks is distributed according to Poisson statistics.

signal follows a Poissonian distribution and presents itself in resolved peaks equally spaced, each one representing the number of photons detected.

The obtained spectrum was then fitted with a multigaussian function, whose parameters were extracted to evaluate the gain at fixed over-voltage.

Waveforms acquired in dark conditions over a wide time window (1 μs) allowed for an estimation of the Dark Count Rate (DCR) by setting an adjustable threshold and counting dark signals occurring in the acquired time window.

The trend of gain and DCR as a function of the OV for 1 × 1 mm^2 SiPMs are reported in Fig. 5, one curve for each of the temperatures tested. Both gain and DCR curves were fitted with a linear function. As can been seen from the plots, gain versus OV shows a uniform behavior with temperature, ranging from $G = (6.0 \pm 0.2) \cdot 10^5$ to $G = (6.1 \pm 0.2) \cdot 10^5$ per over-voltage unit, with a slight increase in the value with lower temperature, as expected. On the other hand, an increasing trend with the temperature can been seen in the DCR plot, as one would expect given the nature of the device.

A comparison between 1 × 1 mm^2 and 6 × 6 mm^2 SiPMs performance in terms of gain per OV unit is shown in Fig. 6. The overall

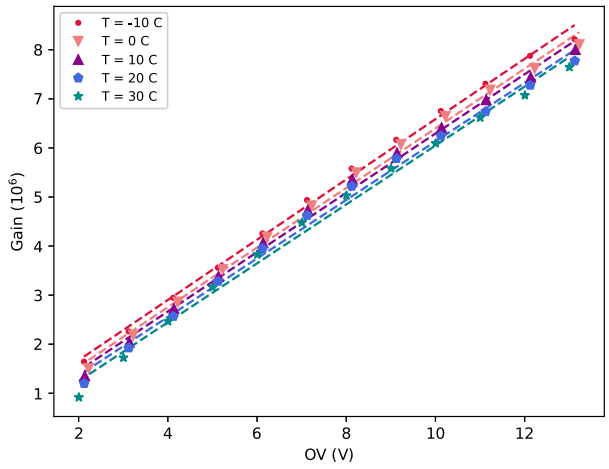

(a) Gain as a function of OV, one curve for each temperature.

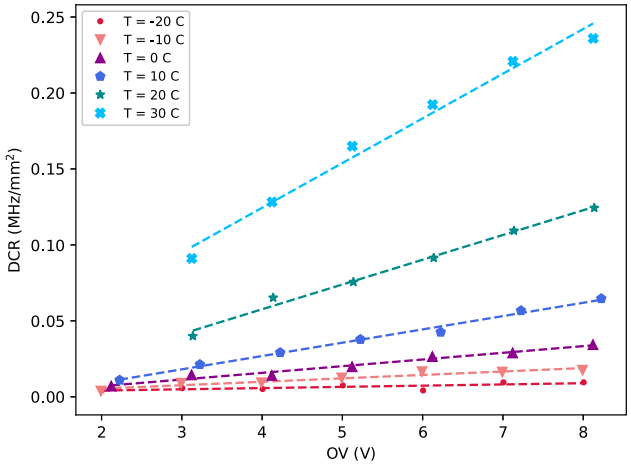

(b) Dark count rate as a function of OV, one curve for each temperature.

Fig. 5. Gain per photo-electron and DCR evaluated for 1 × 1 mm^2 SiPM as a function of the OV applied. Each curve represents data acquired at a fixed temperature.

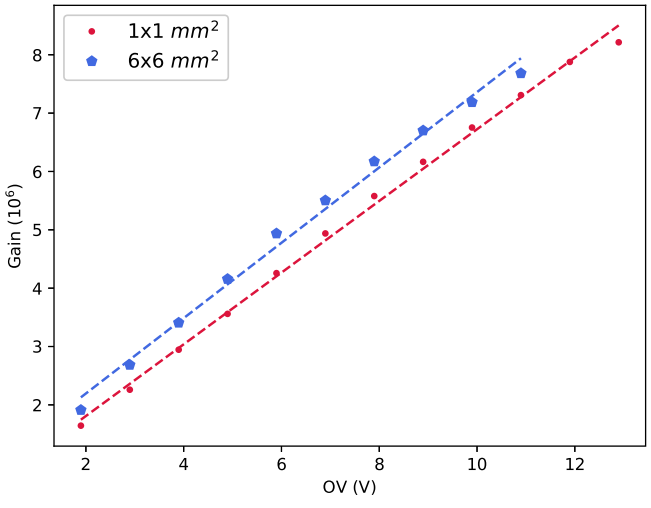

Fig. 6. Comparison between gain of 1 × 1 mm^2 and 6 × 6 mm^2 at a T = −10 °C.

gain per over-voltage unit results are consistent in the two devices tested, with a slightly higher value for the larger device: a value G =

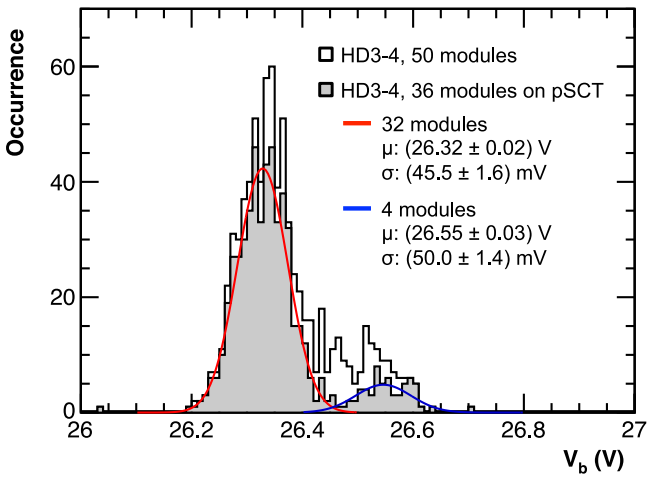

Fig. 7. Breakdown voltages distribution of all the 800 pixels assembled in matrices (white histogram), and of the 576 pixels installed on the pSCT camera (gray histogram). (For interpretation of the references to color in this figure legend, the reader is referred to the web version of this article.)

$(6.1 \pm 0.1) \cdot 10^5$ was found for the 1×1 mm^2 device, while 6×6 mm^2 has $G = (6.4 \pm 0.2) \cdot 10^5$.

4. Upgrade of the photodetection modules of the pSCT camera

During October 2018 a batch of 50 FBK NUV-HD3 SiPM matrices were assembled and electrically characterized at INFN laboratories before the final installation of 36 of them on the pSCT camera, which took place in December 2018. All measurements reported in this section have been carried out at room temperature, T = 25 °C.

The 27×27 mm^2 area printed circuit boards (PCBs) with 0.5 mm distance between sensors were equipped with 16 6×6 mm^2 FBK NUV-HD3 SiPMs. Details on the alignment procedure of the sensors are given in [9].

IV curves were acquired to evaluate the breakdown voltage V_{BD} for each pixel with the fit on the derivative of the logarithm of the current; the overall distribution of the measured breakdown voltages is shown in Fig. 7.

The histogram shows data relative to all the matrices tested (white); data relative to the 36 matrices installed on the pSCT camera are highlighted in gray. A good uniformity can be seen in SiPMs coming from the same Si wafers. The red and blue curves represent the gaussian fit on the distributions of SiPMs installed on the pSCT camera. Data were fitted separately for SiPM coming from different silicon wafer. The spread of the breakdown voltages amounts approximately to 45 mV for 32 modules and to 50 mV for the remaining 4.

After the assembly, tests were conducted with an *ad-hoc* 16-channel front-end electronics to amplify and shape the input signal to match the dynamic range of a CAEN V792 QDC, used to acquire the charge signal of the 16 channels simultaneously over a fixed integration time of 50 ns; see [10] for further details on the development of the front-end electronics.

The uniformity in terms of gain and DCR was verified in order to choose the 36 matrices to equip the camera. Each matrix was tested at different bias voltage V_{BIAS} ranging from 31 V to 36 V, with a 380 nm Pulse Diode Laser switched on and off in turn. An example of a fitted charge distribution at 33 V for 4 neighboring pixels from one matrix is reported in Fig. 8. A multi-gaussian fit is shown superimposed on the data. Although well-resolved, the spectrum here shows a clear decrease in the signal-to-noise ratio with respect to the one reported in Fig. 4. This is expected given the larger size of SiPMs composing the matrices and a higher intrinsic noise of the front-end electronics.

Parameters from the multi-gaussian fit were collected to estimate the integrated charge gain per photo-electron (p.e.) at different over-voltages OV, while data taken under dark conditions were analyzed to evaluate the DCR for each pixel at different OV values. Since it was not possible to acquire single-pixel's waveforms as we did in Section 3, the dark count rate was obtained adopting the following formula:

$$DCR = \frac{N_{tot} - N_0}{N_{tot} \cdot \Delta t}, \tag{2}$$

where N_{tot} is the total number of events acquired, N_0 is the number of event corresponding to the absence of pulses and Δt is the integration time.

The distributions obtained from these values allowed the study of the average performances of the matrices. Plots in Fig. 9 represent the values of gain in ADC units and DCR as a function of the over-voltage

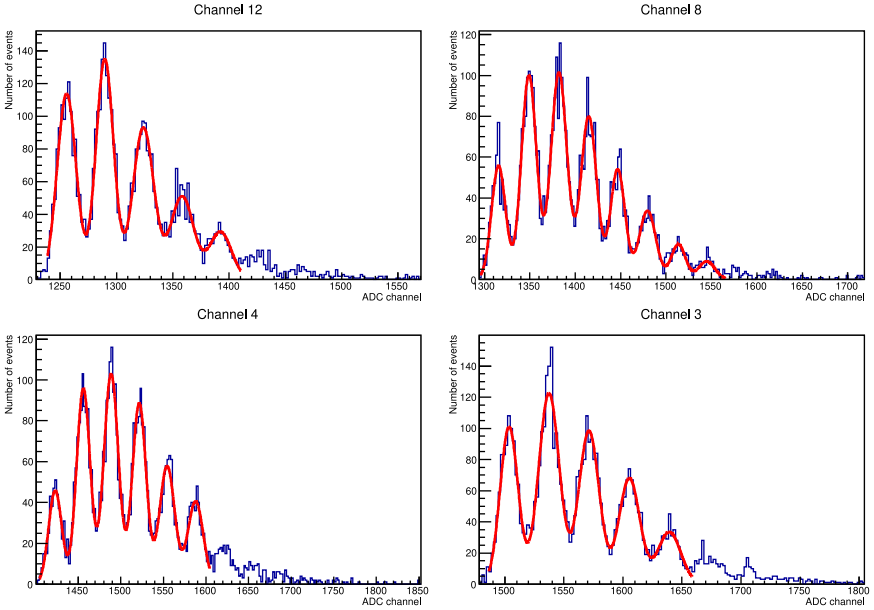

Fig. 8. Charge distribution of the signals of 4 neighboring channels one matrix, biased at 33 V. The integration time is 50 ns. The red line superimposed on data is a multigaussian fit. (For interpretation of the references to color in this figure legend, the reader is referred to the web version of this article.)

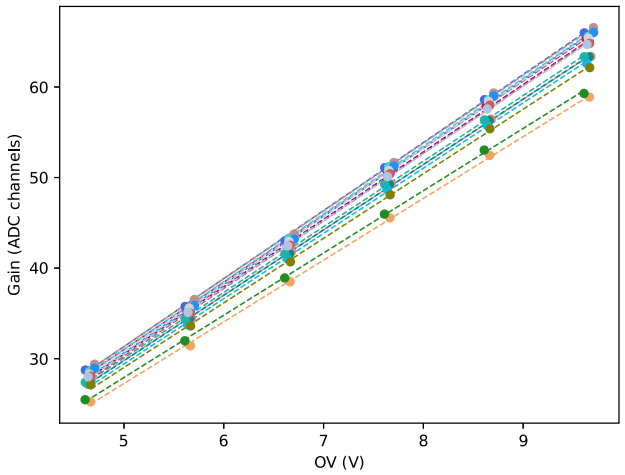

(a) Gain per p.e. as a function of the over-voltage applied.

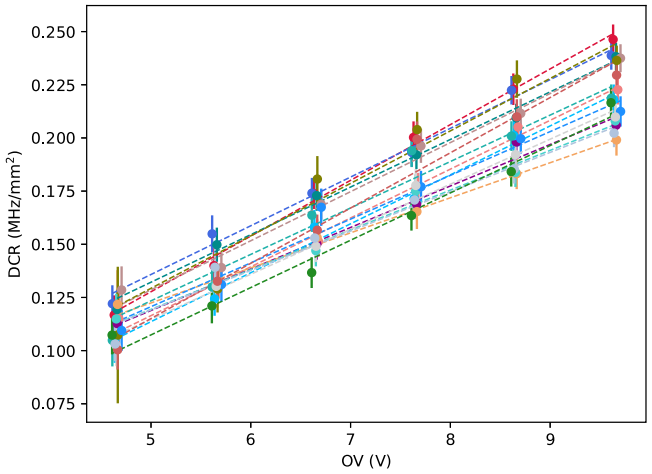

(b) DCR as a function of the over-voltage applied.

Fig. 9. Trend of gain/p.e. (top) and DCR (bottom) for one of the matrices tested. Each curve represents a pixel in the matrix.

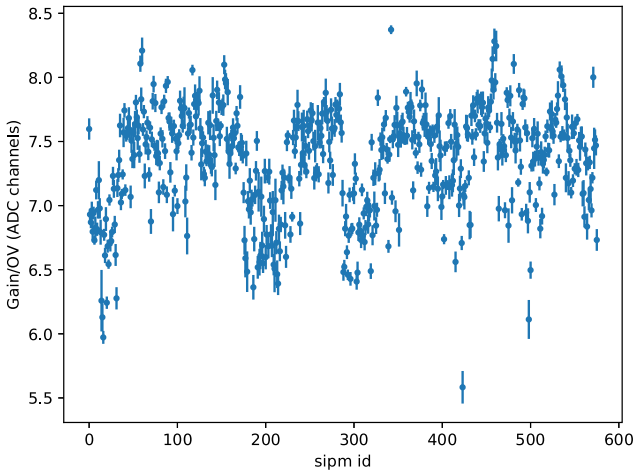

(a)

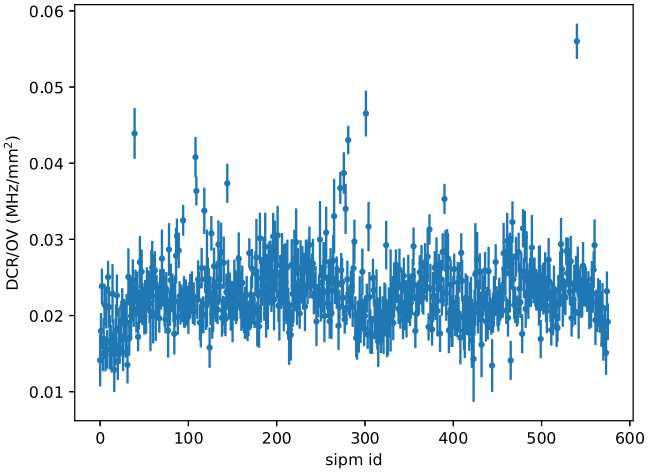

(b)

Fig. 10. Gain (top) and DCR (bottom) per over-voltage unit for the 576 SiPMs installed on the pSCT camera.

for each of the 16 channels in one matrix. The value of the DCR found for SiPM in matrix configuration is compatible with the value reported in Fig. 5(b) for SiPM in single device configuration. The differences are likely to be due to different conditions, such as the temperature at which the measures were carried out.

A linear fit was performed on each curve to obtain the gain and DCR per over-voltage unit, which were estimated from the slope of the best fit line. The estimated parameters' distributions are reported in [11] and show uniformity of 6% and 17% respectively for gain and DCR. Among those tested, 36 matrices showed good and more uniform performances and therefore were selected to be coupled to the front-end electronics of the pSCT camera. In Fig. 10 we report the value of the gain and the DCR per over-voltage unit for the 576 pixels installed on the pSCT camera.

In December 2018, the 36 matrices were aligned on 9 modules using a reference frame with a tolerance of 0.02 mm and specials copper elements. The alignment performed is needed to set the correct curvature in each camera sector. Aligned modules were successfully installed on the pSCT camera at Fred Lawrence Whipple Observatory in Arizona (USA) (see Fig. 11(a), where the INFN modules are in the top-left corner and are highlighted in light blue). The telescope was inaugurated on January 19 2019, and recorded its first event a couple of days later on January 23rd. The image of the event is shown in Fig. 11(b), where INFN modules are in the top-left corner, since this image is facing the sky and it is therefore mirrored with respect to Fig. 11(a).

5. Conclusions and outlooks

According to measurements reported in Sections 3 and 4, SiPM sensors have proved to be suitable to equip the focal plane of Imaging Air Cherenkov Telescope cameras, allowing the performance of the camera to be improved. In particular, measurements reported in Section 4 were fundamental in order to select the sensors to install on the first section of pSCT camera. This section has been equipped with photodetection modules hosting a TARGET–7-based front-end electronics which also hosts a discrete pre-amplifier stage.

A new subfield of the camera will soon be equipped with 25 modules (1600 SiPMs) hosting FBK NUV-HD SiPMs as photodetectors and an upgraded FEE based on the TARGET design. In the new boards, sampling and digitization of the signal will be separated from the trigger circuit in two different ASICs, respectively TARGET–C and the T5TEA, allowing the noise level to be reduced [4,12]. Moreover, the discrete pre-amplifier will be replaced with a new ASIC, the SMART

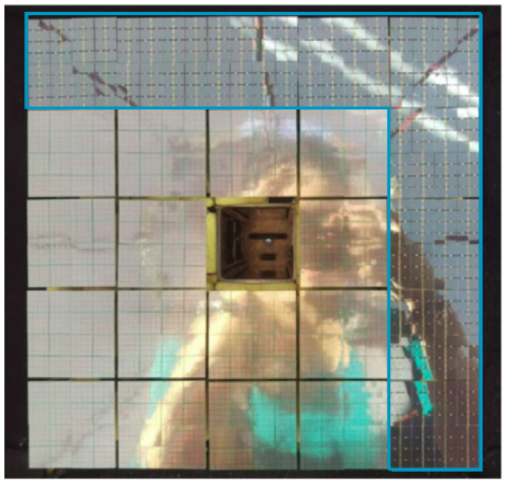

(a) Picture of the sub-field on the camera. 15 HAMAMATSU and 9 FBK modules are installed.The central module was temporarily removed to allocate an alignement module for the telescope pointing procedure and was installed later.

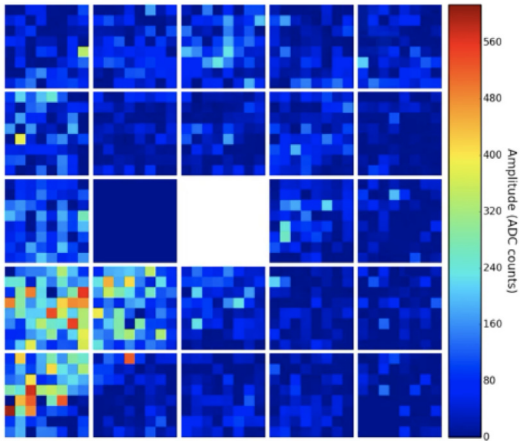

(b) Picture of the first event caught by the prototype of the Schwarzschild–Couder Telescope on January 23 2019. The image shown faces the sky and it is therefore mirrored with respect to 11a.

Fig. 11. Picture of the pSCT camera (top) and first event caught by the telescope (bottom). (For interpretation of the references to color in this figure legend, the reader is referred to the web version of this article.)

(SiPM Multichannel Asic for high Resolution Cherenkov Telescopes) designed by INFN to exploit the integrated technology [13]. The amplification stage is characterized by a configurable gain stage, followed by a tail suppression and signal shaping stage, with an adjustable filtering frequency. Both gain and shaping time can be optimized by the user with a Digital-to-Analog Converter (DAC).

The new upgrades will lead to an improvement on the performance of the camera, maximizing the field of view and achieving a lower trigger threshold, allowing the pSCT to start a physics campaign. The full pSCT camera consisting of 177 modules and a total of 11328 pixels is planned to be fully equipped within the next few years.

Declaration of competing interest

The authors declare that they have no known competing financial interests or personal relationships that could have appeared to influence the work reported in this paper.

References

[1] M. Actis, et al., Design concepts for the Cherenkov Telescope Array CTA: an advanced facility for ground-based high-energy gamma-ray astronomy, Exp. Astron. 32 (3) (2011) 193–316, http://dx.doi.org/10.1007/s10686-011-9247-0.

[2] K.J. Meagher, Schwarzschild-Couder Telescopefor the Cherenkov Telescope Array, in: Proceedings, SPIE Astronomical Telescopes + Instrumentation 2014: Ground-based and Airborne Telescopes, 2014, http://dx.doi.org/10.1117/12.2054979, arXiv:1407.3271.

[3] N. Otte, et al., Development of a SiPM Camera for a Schwarzschild-Couder Cherenkov Telescope for the Cherenkov Telescope Array, in: Proceedings, 34th International Cosmic Ray Conference, ICRC 2015: The Hague, The Netherlands, July 30-August 6, 2015, PoS ICRC2015, 2016, p. 1023, http://dx.doi.org/10.22323/1.236.1023.

[4] R. Paoletti, The upgraded camera for the prototype Schwarzschild-Couder Telescope of the Cherenkov Telescope Array, in: T.B. Hull, D.W. Kim, P. Hallibert (Eds.), in: Astronomical Optics: Design, Manufacture, and Test of Space and Ground Systems II, vol. 11116, International Society for Optics and Photonics, SPIE, 2019, pp. 73–79, http://dx.doi.org/10.1117/12.2530431.

[5] L. Tibaldo, et al., in: Proceedings, 34th International Cosmic Ray Conference, ICRC 2015: The Hague, The Netherlands, July 30-August 6, 2015, PoS ICRC2015, 2016, p. 932, [34, 932(2015)]. arXiv:1508.06296.

[6] K. Bechtol, et al., Astropart. Phys. 36 (2012) 156–165, http://dx.doi.org/10.1016/j.astropartphys.2012.05.016, arXiv:1105.1832.

[7] G. Ambrosi, et al., in: SPIE 2017 Proceedings, vol. 10392, 2017, p. 40, URL https://spie.org/Publications/Proceedings/Paper/10.1117/12.2272982.

[8] C. Adams, et al., Development and operations of INFN optical modules for the SCT Telescope camera proposed for the Cherenkov Telescope Array Observatory, 2019, arXiv e-prints arXiv:1909.08361.

[9] G. Ambrosi, et al., Nucl. Instrum. Methods A 845 (2017) 8–11, http://dx.doi.org/10.1016/j.nima.2016.04.050, Proceedings of the Vienna Conference on Instrumentation 2016. [link]. URL http://www.sciencedirect.com/science/article/pii/S0168900216302558.

[10] G. Ambrosi, et al., SiPM and front-end electronics development for Cherenkov light detection, in: Proceedings, 34th International Cosmic Ray Conference, ICRC 2015: The Hague, The Netherlands, July 30-August 6, 2015, PoS ICRC2015, 2016, p. 992, http://dx.doi.org/10.22323/1.236.0992, arXiv:1509.03207.

[11] G. Ambrosi, et al., Characterization and development of NUV SiPMs for INFN optical modules for the SCT Medium Size Telescope proposed for the CTA Observatory, in: 2019 IEEE 8th International Workshop on Advances in Sensors and Interfaces, IWASI, 2019, pp. 37–41.

[12] S. Funk, et al., TARGET: A digitizing and trigger ASIC for the Cherenkov telescope array, AIP Conf. Proc. 1792 (1) (2017) 080012, http://dx.doi.org/10.1063/1.4969033, arXiv:1610.01536.

[13] C. Adams, et al., Characterization and assembly of near-ultraviolet SiPMs for the Schwarzschild-Couder medium-size telescope proposed for the CTA Observatory, in: R.B. James, A. Burger, S.A. Payne (Eds.), in: Hard X-Ray, Gamma-Ray, and Neutron Detector Physics XXI, vol. 11114, International Society for Optics and Photonics, SPIE, 2019, pp. 52–60, http://dx.doi.org/10.1117/12.2530617.